Plasma Sources Sci. Technol. **19** (2010) 034018 (7pp) doi:10.1088/0963-0252/19/3/034018

Large-area high-density helicon plasma sources

S Shinohara[1], T Motomura[1], K Tanaka[1], T Tanikawa[2] and K P Shamrai[3]

[1] Interdisciplinary Graduate School of Engineering Sciences, Kyushu University, Japan
[2] Research Institute of Science and Technology, Tokai University, Japan
[3] Institute for Nuclear Research, National Academy of Sciences of Ukraine, Kiev, Ukraine

E-mail: sinohara@aees.kyushu-u.ac.jp

Received 28 July 2009, in final form 12 October 2009
Published 21 May 2010
Online at stacks.iop.org/PSST/19/034018

Abstract
High-density (10^{12}–10^{13} cm^{-3}) helicon plasmas produced using two different but similar devices whose diameters are very large, 40 cm and 74 cm, respectively, have been characterized. A scaling of the particle production efficiency has been investigated in detail into a low aspect ratio (the ratio of the diameter to the axial length) region down to 0.075. It has been found that reducing this ratio manifests the standing wave-like patterns of the excited radio frequency (rf) fields. Spatial profiles of the electron density and the rf wave fields are measured, showing the effectiveness of the control of these profiles by changing the magnetic field configurations near the excitation antenna. Finally, high-beta plasmas with up to $\beta \sim 0.8$, that exhibit diamagnetic character, where β is the ratio of the plasma pressure to the magnetic pressure, have been produced with low magnetic fields.

(Some figures in this article are in colour only in the electronic version)

1. Introduction

Helicon plasma sources [1–5] using a radio frequency (rf) wave have been extensively utilized because of the ability to produce high-density (up to more than 10^{13} cm^{-3}) plasmas with a high ionization degree (up to more than several tens percent) in a wide range of external control parameters. Thus, helicon sources can be useful in fundamental research and various applications, such as materials processing, nuclear fusion, gas lasers, space plasma modelling and plasma acceleration/propulsion.

Although large-area plasma sources are important in many fields mentioned above, large-area, high-density helicon sources with diameters exceeding 10–20 cm have been rarely examined in spite of their great potentiality in many fields. Recent research efforts have shown that the use of a flat spiral antenna located behind a quartz window to realize a large-diameter helicon plasma [6–14] can achieve a much higher plasma production efficiency [9, 10, 13] when compared with the standard antenna configuration, in which an antenna is wound around a quartz tube, to construct a helicon source. The use of a flat spiral antenna also enables us to easily reduce the aspect (axial length-to-diameter) ratio A of a plasma by simply reducing the device axial length. Low aspect ratio plasmas are particularly useful, for industrial [15] and propulsion [16, 17] applications. However, examining the plasma production scaling (generally particle confinement will be expected to become poorer when the axial length is reduced) as well as the rf wave characteristics (axial boundary conditions may play important roles) with a short axial length is not enough [13, 14]. Investigating how the plasma density profiles, especially the radial density profiles, can be controlled is very important to technologically advance the various plasma applications.

Utilizing the advantage of the wide operational range of the external magnetic field strength, high-beta high-density helicon plasmas [18, 19] have also been investigated in a low field regime. Here, the beta β is defined as the ratio of the plasma pressure p to the magnetic pressure $B^2/2\mu_0$ (B: magnetic field in the vacuum, μ_0: permeability in the vacuum). High-beta plasmas, in which the interaction between the plasma and magnetic fields is of fundamental interest, can supply many challenging topics, such as the strong diamagnetism and associated instabilities observed in space [20] and laboratory [21] plasmas, including nuclear fusion plasmas [22]. However, these phenomena have not been clearly understood.

In this paper, we present the discharge performance, focusing on the plasma production efficiency, of the newly

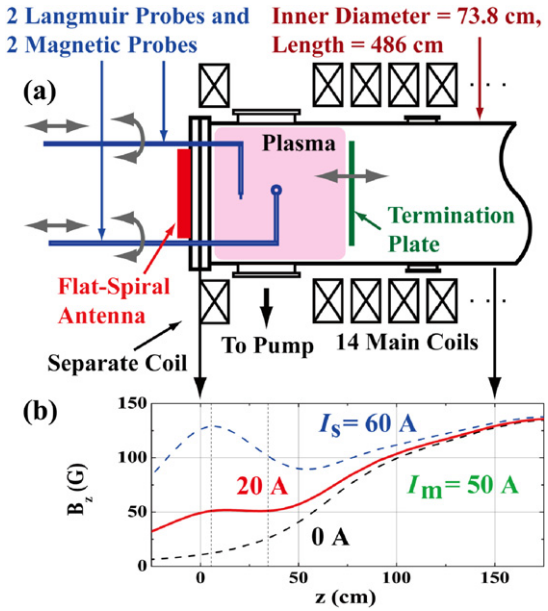

Figure 1. (*a*) Schematic of LHPD at ISAS, JAXA. (*b*) Axial magnetic field configurations for various values of the separate coil current I_s for constant I_m of 50 A.

developed large-area, high-density helicon plasma sources. The way to control the radial density profile and the characteristics of excited helicon waves with short axial lengths are also described. Finally, the results of a trial experiment to investigate the diamagnetic effect in a high-beta plasma are presented. In our experiments described in this paper, we have utilized two large-area helicon devices: large helicon plasma device (LHPD) [9–14], whose inner vessel diameter and axial length are 74 cm and 486 cm, respectively, at the Institute of Space and Astronautical Science (ISAS), Japan Aerospace eXploration Agency (JAXA) and Large-Diameter Device (LDD) at Kyushu University [23], whose inner vessel diameter and axial length are 40 cm and 126 cm, respectively.

2. LHPD Experiment

2.1. Experimental setup

Our experiments at ISAS, JAXA are performed using the LHPD [9–14], which has the world's largest helicon plasma volume of 2.1 m^3 with the world's largest diameter of 74 cm, as far as we know, as shown in figure 1(*a*). In order to shorten the axial plasma length, we have installed an electrically floating termination plate [13, 14] made of a stainless steel (SUS) punching plate. A uniform magnetic field in the central region (over 2 m in the axial direction) is produced by the 14 main coils. The main coil current I_m is 50 A in the experiments described in this paper, which corresponds to 140 G. In order to compensate the weak magnetic field near the spiral antenna, a separate coil is additionally installed (see the left-hand side of the chamber in figure 1(*a*)). The separate coil current I_s can be varied, so that different magnetic field configurations near the antenna can be easily obtained (see figure 1(*b*)).

The base pressure is $\sim 10^{-7}$ Torr, and the typical working gas is argon (Ar) with a fill pressure P_{Ar} of

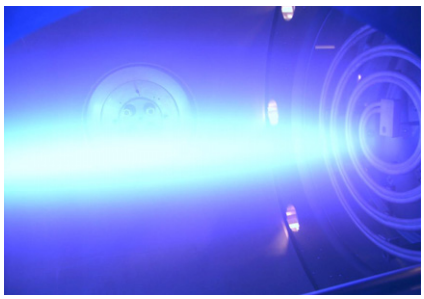

Figure 2. Photo taken from the observation port at $z = 31.5$ cm (see figure 1(*a*)) near the spiral antenna with $I_s = 60$ A and $P_{inp} \sim 2.5$ kW ($L = 486$ cm).

0.75–7.5 mTorr (0.75 mTorr is used unless specified otherwise in our experiments). The rf system [9] used is as follows. The spiral antenna, which is expected to excite the azimuthal mode number of $m = 0$ and is installed outside the vacuum chamber, has 4 turns with 43 cm outer diameter. The maximum output power of the rf amplifier is 5 kW at a typical frequency of 7 MHz. Plasma is produced repetitively with a typical discharge pulse width of 12–40 ms with the repetition rate of 1 Hz.

The spatial plasma parameters, such as the electron density n_e and the electron temperature T_e (typically 3–5 eV), are measured by axially and radially scanning two Langmuir probes. The excited rf wave field patterns are measured by using two one-turn magnetic probes. These probes inserted from the end flange (antenna side (see figure 1(*a*))) can also measure the radial as well as axial profiles. Ordinary digital cameras are used to monitor the plasma light emission.

2.2. Plasma production and scaling

Figure 2 shows a typical example of the helicon plasma light emission. In this particular example, the input rf power is $P_{inp} \sim 2.5$ kW and the full axial plasma length of $L = 486$ cm (without the termination plate) is used. In figure 2, the spiral antenna outside the quartz window is seen on the right-hand side, and in the central region of the plasma, we can clearly see the so-called blue mode, which is one of the indicators of a high-density helicon plasma established after the density jump from the inductively coupled plasma (ICP). Generally, this blue mode structure, whose emission is considered to mostly come from Ar II lines, is spindle shape. The diameter and extent of this spindle depend on the magnetic field configuration, e.g. the convergent field towards the main chamber makes a smaller radius, and on the rf power, i.e. plasma density. The typical diameter of the structure is 10–20 cm, which is smaller than the diameters of the spiral antenna and plasma, with an axial length exceeding 1 m.

At various positions of the termination plate, we have measured the electron density n_e using two devices of the LHPD and the LDD (this device will be described later in section 3.1). After the density jump, we can find a gradual decrease in n_e as the plasma length L is reduced for the same input rf power [13, 14]. However, a plasma with $n_e \sim 10^{12}$ cm^{-3} can still be produced even with L as short as 5.5 cm

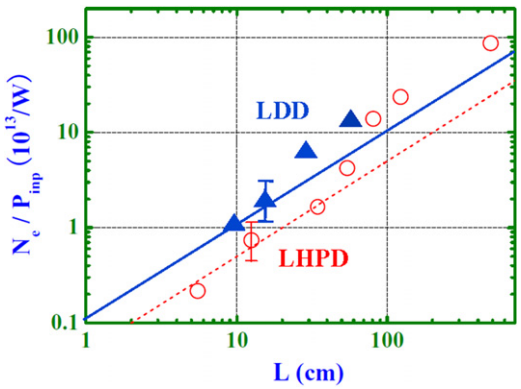

Figure 3. Relationship between N_e/P_{inp} and L from LHPD (open circles) and LDD (closed triangles). Here, linear curves are also shown.

[13] in the LHPD, i.e. $A = 0.075$. This value of A is much less than that of A in conventional devices, which is typically well over unity (the minimum value obtained so far was ∼0.5 [7]). In a low aspect ratio plasma, we have observed a standing wave-like pattern for the excited helicon mode, which will be described later.

Figure 3 shows the plasma production efficiency N_e/P_{inp} as a function of L whose value is varied by changing the position of the termination plate, where N_e is the total number of electrons in the plasma. From the simple calculation [10] of the balance between the plasma loss power and the input power, we can expect that N_e/P_{inp} is proportional to L (in the short L region), where the dominant particle loss is along the z-axis. The two data sets from two different devices, namely the LHPD and the LDD, follow a similar scaling law, $N_e/P_{inp} \propto L$, as long as L is less than a few tens of centimetres. It should be noted that the value of the proportionality coefficient for the ideal case is larger than the experimentally obtained values by a factor of 2–3. From figure 3, it can be seen that the plasma production efficiency for the LDD is better than that for the LHPD. This may be due to the fact that the higher Ar pressure P_{Ar} is used in the LDD experiments than in the LHPD ones, which leads to a higher plasma density in the LDD than in the LHPD.

2.3. *Density profiles and wave characteristics*

As was shown in [9], the radial electron density profile can be controlled by changing the magnetic field configurations. Here, in order to see this effect in more detail, we have measured the two-dimensional density profiles by changing I_s, as shown in figure 4. With the increase in I_s (e.g. from figures 4(*a*) to 4 (*b*)), which corresponds to less convergent field towards the main chamber (see figure 1(*a*)), the central electron density (∼10^{12} cm^{-3}) becomes lower and a broader radial profile is observed. Figure 4(*a*) also shows that the plasma radius shrinks with z ($z > 40$ cm) due to the convergent magnetic field effect, in contrast to figure 4(*b*) that the plasma radius changes little in the region of $z > 40$ cm under the nearly uniform field. These behaviours can be understood by the fact that the plasma is produced by the rf wave (the plasma production region is along the magnetic field lines, as

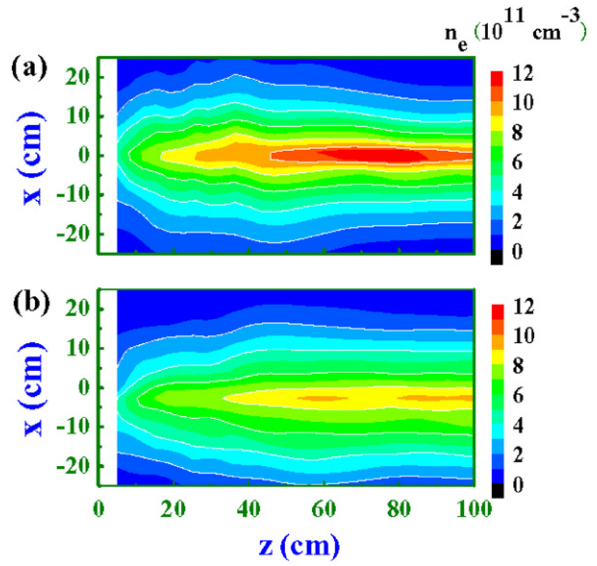

Figure 4. Contours of the electron density in the case of (*a*) $I_s = 20$ A and (*b*) 60 A with $P_{inp} \sim 2.5$ kW ($L = 486$ cm).

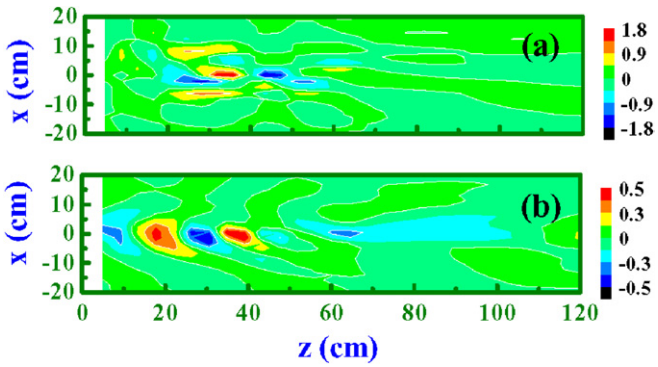

Figure 5. Contours of the normalized rf magnetic field B_z/I_A in the case of (*a*) $I_s = 20$ A and (*b*) 60 A with $P_{inp} \sim 2.5$ kW ($L = 486$ cm).

is described in the next paragraph) and the generated plasma flows nearly along the field lines.

Concerning the rf plasma production influenced by the magnetic field configuration, two-dimensional profiles of the rf fields of excited waves are measured to examine the helicon wave propagation, as shown in figure 5 under the same experimental conditions for figure 4. Here, the ratio of the excited rf magnetic field B_z (axial component) to the amplitude of the rf antenna current I_A is shown (in colour code), changing the magnetic field configurations. With the decrease in I_s (e.g. from figures 4(*b*) to (*a*)), the rf wave propagates towards the inner region of the plasma column, indicating that the wave propagation is along the magnetic field line (see figure 1(*b*)). Since the wave energy density is roughly proportional to the rf component of the B_z^2 from [25], the plasma production region reflects this wave profile. Therefore, the rf wave profiles in figure 5 are consistent with the obtained density profiles of figure 4. Note that while the fundamental radial mode (the Bessel function J_0 like [1–5]) with the axial wavelength of ∼20 cm is observed for the case of nearly uniform magnetic field (figure 5(*b*)), the complicated wave structures with a

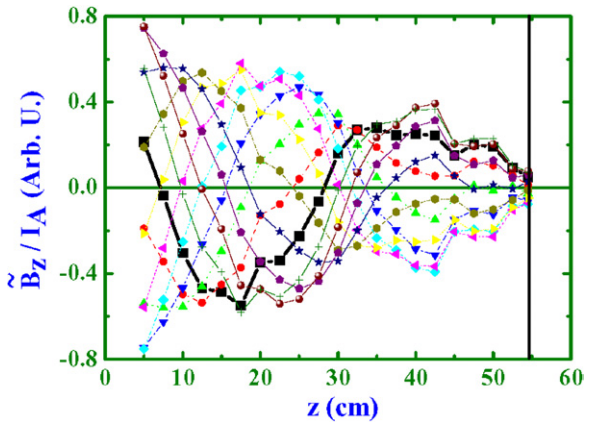

Figure 6. Axial profiles of the normalized rf magnetic field B_z/I_A in the case of $I_s = 60$ A with $P_{inp} \sim 3.3$ kW ($L = 54.5$ cm) at 12 phases in one rf period.

mixture of the higher radial modes [13, 14] are observed in the case of convergent field (figure 5(*a*)). Clarifying these phenomena is left for future study.

In order to investigate the effect of axial boundaries on the wave structures in short axial cases, where the axial wavelength is comparable to the axial plasma length L, we have shortened L down to 5.5 cm. As shown in figure 6 ($L = 54.5$ cm case), the excited rf field B_z normalized by I_A shows a standing wave-like pattern with the axial mode number n, which is the ratio of L to the wavelength, ∼5/4. This is consistent with the expectation that an ideal n of helicon waves should be $(1/4) + (1/2)\,p$, where p is zero or positive integer [13, 14, 24], as a result of a partial reflection of the helicon wave at the termination plate and the excitation of the surface wave at the plasma-quartz window interface.

3. LDD Experiment

3.1. Experimental setup

Experiments at Kyushu University using the newly developed LDD [23], which has a four-turn spiral antenna [7, 8], as shown in figure 7, are carried out with P_{Ar} of 2–10 mTorr (the base pressure $\sim 10^{-6}$ Torr). Here, the maximum rf output power is 5 kW at a frequency of 7 MHz, and a typical discharge pulse width is 10 ms with 10 pulses per second.

In order to investigate the effects of the magnetic field configurations on the plasma performance, the 8 magnetic coils are energized with two separate power supplies, so that one can easily obtain various field configurations such as the uniform, divergent and convergent field configurations. The axial plasma size L can be varied by the movable termination (SUS) plate. Plasma parameters (rf wave structures) are measured by Langmuir probes (magnetic probes). Typical electron density and electron temperature are 10^{12}–10^{13} cm^{-3} and 3–5 eV, respectively. Plasma light emission is monitored by the high-speed (up to 1200 fps) digital camera (CASIO EX-F1).

3.2. Plasma production and density profiles

In figure 8, the features of light emission from the helicon plasma taken by the high-speed camera under three magnetic field configurations are compared. Here, the ratios of the maximum field B_{max} (∼50 G) to the minimum field B_{min} in the plasma region (z is from 0 to 60 cm with $L = 60$ cm) in the cases of the divergent, the uniform and the convergent fields are 9.4, 1 and 1.8, respectively. In each frame, the top (bottom) is towards the plasma source region (the termination end plate) which corresponds to the left-hand (right-hand) side of the device in figure 7. Similarly, the right (left) side corresponds to the direction of the device bottom (top). An open circle with a small closed circle in each frame indicates a gauge port located on the opposite side of the vacuum vessel.

From these pictures, it can be seen that there are so-called blue modes towards the source side in the cases of the convergent and uniform magnetic field configurations. In addition, the convergent (divergent) field appears to make the plasma light focus into (defocus out of) the central radial region of the device towards the direction to the end plate; in other words the convergent (divergent) field makes the radial plasma density profile peaked (broader). This feature is consistent with the results of the LHPD experiments described in section 2.3 and also with the present probe measurements, as shown in figure 9(*b*). From this figure, the values of the full width at half maximum in the cases of divergent, uniform and convergent magnetic fields are 22 cm, 19 cm and 16 cm, respectively, and the electron density n_e in the case of divergent field configuration is lower than those in the other two cases. Here, $B_a \sim 50$ G is the magnetic field at $z = 0$ cm (near the antenna), and the ratios of B_{max} to B_{min} in the cases of the divergent, uniform and convergent field configurations are 9.4, 1 and 1.3, respectively.

Next, we investigate the plasma performance as a function of the axial plasma length L. In the case of $L = 30$–125 cm, n_e gradually decays with z except for the region near the termination plate, where an abrupt drop in the density is observed. The electron density n_e itself does not change very much with decreasing L (see figure 9(*a*) and figure 10 in the cases of $L = 60$ and 30 cm, respectively). Further reduction in L, as is shown in figure 10, causes the lower n_e, but a high electron density of $n_e \sim 10^{13}$ cm^{-3} can still be obtained even with $L \sim 10$ cm, which corresponds to $A = 0.25$. Note that no high-density stable discharges can be obtained when $L < 9.5$ cm.

The higher electron density (than the LHPD case) achieved here can result from the smaller plasma diameter of the LDD (n_e is expected to be proportional to P_{inp}/a^2 from [10], where a is the plasma radius) and a higher gas pressure used for the LDD experiments (a higher argon neutral pressure tends to generate a higher electron density plasma as was mentioned). As shown in figure 3, the LDD results in the short axial length cases also indicate the linear scaling of plasma production efficiency with L, which is in accordance with the discussion in [10].

3.3. Initial attempt of high-beta plasma production

As was mentioned before, high-beta plasmas can supply many challenging topics, since the strong interaction between the

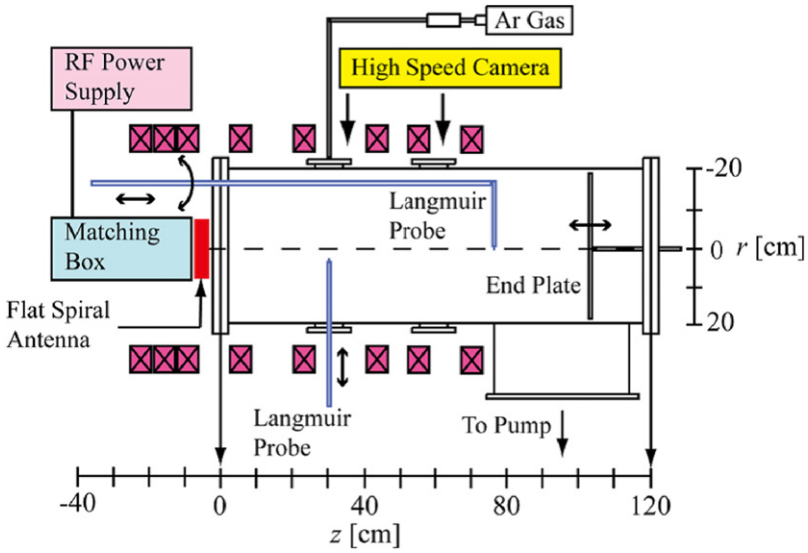

Figure 7. Schematic of LDD at Kyushu University.

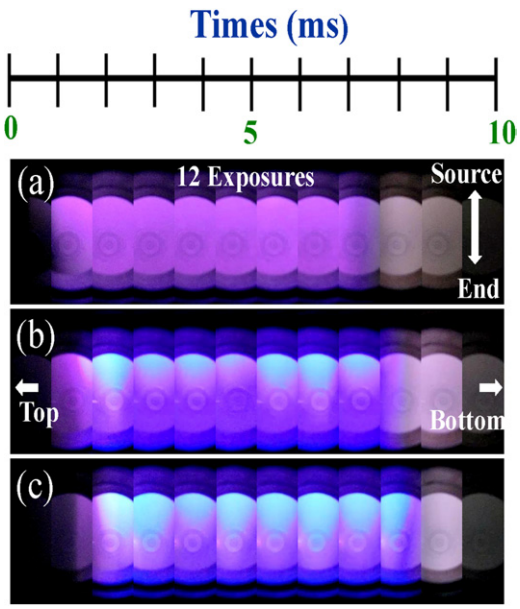

Figure 8. Time evolutions of plasma light taken from the observation port at $z = 30$ cm (see figure 7) under (a) the divergent, (b) the uniform and (c) the convergent magnetic field configurations with $B_{max} \sim 50$ G, $P_{Ar} = 10$ mTorr and $P_{inp} \sim 2.5$ kW ($L = 60$ cm).

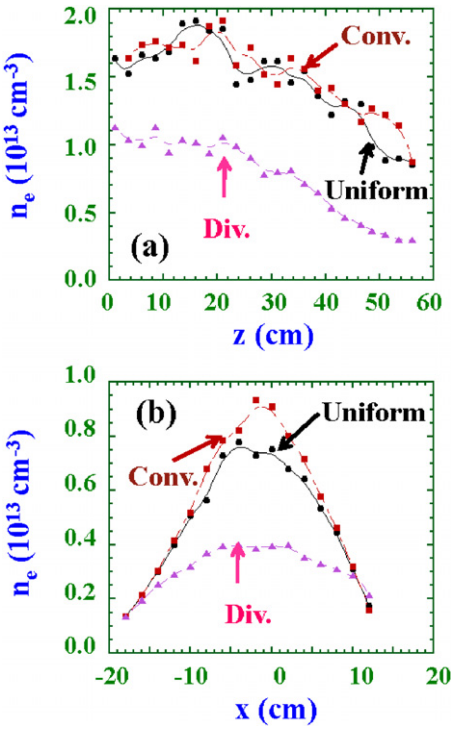

Figure 9. (a) Axial and (b) radial profiles of the electron density n_e under the three magnetic field configurations with $B_a \sim 50$ G, $P_{Ar} = 10$ mTorr and $P_{inp} \sim 2$ kW ($L = 60$ cm).

plasma and the magnetic field causes the peculiar magnetic structure accompanied by instabilities. In addition, the production of high-beta plasmas can be highly efficient because of the low external magnetic field and the high plasma pressure. This means that a power supply to generate the external magnetic field can be small in size and light weighted, which is a significant practical advantage.

Since we can create a high-density plasma of $\sim 10^{13}$ cm^{-3} even under the low magnetic field of several tens of gauss, an attempt has been made if the diamagnetic effect could be observed in the plasma under this condition. Figure 11(a) shows the central electron beta β_0 in the argon pressure P and the magnetic field B space. The range of high β_0 obtained is between 0.4 and 0.8. Here, β_0 is the ratio of the electron pressure measured at the plasma centre ($x = 0$ cm) with $z = 30$ cm to the vacuum magnetic field pressure, and the electron pressure generally exceeds the ion pressure. Figure 11(b) shows the decrement in the magnetic field ΔB, i.e. the decrease in the magnetic field strength from the vacuum one, in the same (P, B) space. The range of ΔB obtained here is between 0.8 and 2.6 G.

Now, we will discuss the diamagnetic effect observed. From figure 11, with the increase in B, β_0 decreases while ΔB

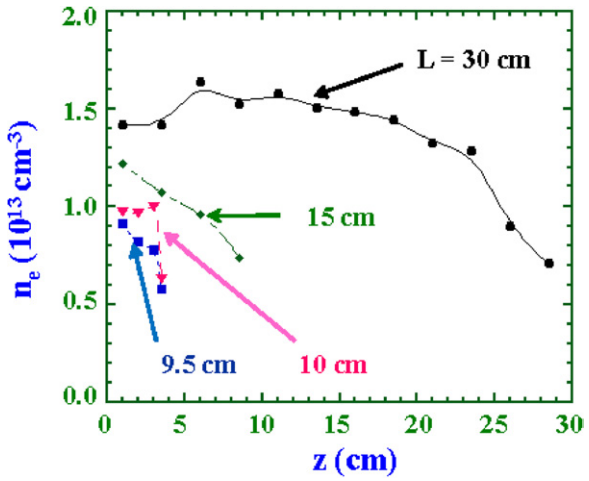

Figure 10. Axial profiles of the electron density n_e by changing the axial plasma length L with the uniform magnetic field of 50 G with $P_{Ar} = 10$ mTorr and $P_{inp} \sim 2$ kW.

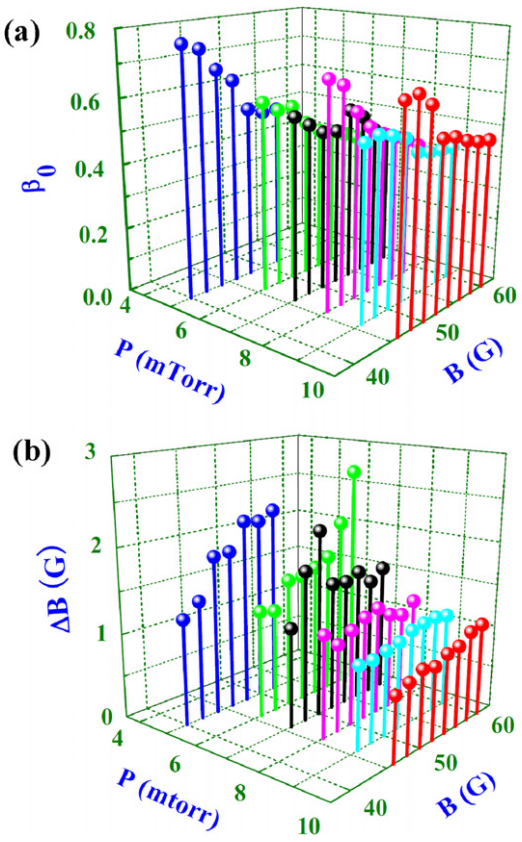

Figure 11. (*a*) Central electron beta β_0 and (*b*) decrement in the magnetic field ΔB in (argon pressure P, magnetic field B) space under the uniform magnetic field with $P_{inp} \sim 2$ kW ($L = 60$ cm).

increases, as expected. β_0 decreases because β_0 is inversely proportional to B^2 by definition and n_e changes little with B. ΔB increases because ΔB is roughly proportional to B if the diamagnetic effect does not change very much with B in this limited range. From figure 11(*b*), ΔB increases with the decrease in P. This may be related to the Hall parameter effect discussed later.

Generally speaking, the constancy of the total pressure (the so-called magnetohydrodynamic (MHD) condition), i.e. the sum of the plasma and the magnetic pressures, holds good [21, 26, 27] in the case of (i) the Larmor radius is much less than the plasma radius, (ii) the Hall parameter $\omega_c\tau \gg 1$ (ω_c: angular cyclotron frequency, τ: collision time) and (iii) the characteristic time of the plasma discharge is much shorter than the magnetic diffusion time $\tau_B \sim \mu_0\sigma a^2$ (σ: conductivity). In our case, the maximum diamagnetic ratio of $\Delta B/B$ is 0.045, while the ideal MHD condition predicts ~0.5, which is one order of magnitude larger than the observed value.

We will discuss the reason for this discrepancy. (i) The maximum ion Larmor radius, which is much larger than the electron one, is several centimetres, which is smaller than the plasma radius of 20 cm. (ii) The electron Hall parameter is much larger than unity, but the ion Hall parameter is estimated to be slightly smaller than unity, using the ion–neutral collision frequency, which is proportional to the argon pressure P. (iii) τ_B is on the order of 0.1 ms, while the discharge time τ_D is 10 ms. From these conditions, the ion diamagnetic effect is small because of the violation of the MHD condition (ii) and the smaller ion temperature compared with the electron one. The large electron diamagnetic effect can be expected in the case of the high beta value from conditions (i) and (ii). However, the total diamagnetic field is also small due to the fact that τ_B is shorter than τ_D from condition (iii), which may be the major effect on the reduction in the diamagnetic effect. In fact, this effect was found to be smaller ($\Delta B/B \sim 0.02$) than our results due to the smaller a of 9 cm [19] with the other parameters nearly the same as ours except for the lower pressure of 1 mTorr.

4. Conclusions

High-density (10^{12}–10^{13} cm^{-3}) helicon plasmas using spiral antennas in two devices, the LHPD and the LDD, whose inner diameters are very large values of 40 cm and 74 cm, respectively, have been characterized. A scaling of the particle production efficiency N_e/P_{inp}, which is proportional to the axial length L, has been discussed in a low aspect ratio region down to $A = 0.075$, by the use of the termination plates. In short L cases, the conditions imposed by the axial boundaries force the excited rf to fields form standing wave-like patterns. Spatial profiles of the density and the rf wave fields are measured, showing the effectiveness of the control of these profiles by changing the magnetic field configurations (such as the uniform, divergent and convergent field ones) near the excitation antenna. Finally, high central electron beta plasmas with up to $\beta_0 \sim 0.8$ have been produced with the low magnetic field of several tens of gauss. These plasmas exhibit a small diamagnetic effect ($\Delta B/B$ is less than 0.045), and the result obtained is discussed from the MHD viewpoint.

Acknowledgments

Our LHPD experiments were conducted in and supported by the Space Plasma Laboratory at ISAS, JAXA under their research collaboration programme. The authors would like

to thank Dr I Funaki, Dr S Sato, Dr T Takeda and Professor K Yamagiwa for their assistance in carrying out the LHPD experiments. This work has been partly supported by the Grants-in-Aid for Scientific Research (A) contract #17206084, (B) #20340163 and (C) 19540524 from the Japan Society for the Promotion of Science.

This paper is dedicated to the memory of late Professor K Toki.

References

[1] Boswell R W 1970 *Phys. Lett.* A **33** 457
[2] Shinohara S 1997 *Japan. J. Appl. Phys.* **36** 4695 and references therein (review paper)
[3] Boswell R W and Chen F F 1997 *IEEE Trans. Plasma Sci.* **25** 1229 and references therein
[4] Chen F F and Boswell R W 1997 IEEE *Trans. Plasma Sci.* **25** 1245 and references therein
[5] Shinohara S 2002 *J. Plasma Fusion Res.* **78** 5 and references therein (in Japanese)
[6] Stevens J E, Sowa M J and Cecchi J L 1995 *J. Vac. Sci. Technol.* A **13** 2476
[7] Shinohara S, Takechi S and Kawai Y 1996 *Japan. J. Appl. Phys.* **35** 4503
[8] Shinohara S, Takechi S, Kaneda N and Kawai Y 1997 *Plasma Phys. Control. Fusion* **39** 1479
[9] Shinohara S and Tanikawa T 2004 *Rev. Sci. Instrum.* **75** 1941
[10] Tanikawa T and Shinohara S 2004 *Proc. Int. Congress on Plasma Physics (Nice, France)* ccsd-00002013
[11] Shinohara S and Tanikawa T 2005 *Phys. Plasmas* **12** 044502
[12] Tanikawa T and Shinohara S 2006 *Thin Solid Films* **506–507** 559
[13] Shinohara S, Hada T, Motomura T, Tanaka K, Tanikawa T, Toki K, Tanaka Y and Shamrai K P 2009 *Phys. Plasmas* **16** 057104
[14] Motomura T, Tanaka K, Shinohara S, Tanikawa T and Shamrai K P 2009 *J. Plasma Fusion Res. Ser.* **8** 7
[15] Lieberman M A and Lichtenberg A J 1994 *Principles of Plasma Discharges and Materials Processing* (New York: Wiley)
[16] Jahn R G 1968 *Physics of Electric Propulsion* (New York: McGraw-Hill)
[17] Charles C 2009 *J. Phys D: Appl. Phys.* **42** 163001
[18] Scime E E, Keiter P A, Balkey M M, Boivin R F, Kline J L and Blackburn M 2005 *Phys. Plasmas* **7** 2157
[19] Corr C S and Boswell R W 2007 *Phys. Plasmas* **14** 122503
[20] Kivelson M G and Russel C T 1995 *Introduction to Space Physics* (Cambridge: Cambridge University Press)
[21] Stenzel R L and Urrutia J M 2000 *Phys. Plasmas* **7** 4450
[22] Sykes A 1997 *Phys. Plasmas* **4** 1665
[23] Tanaka K, Motomura T, Murakami K and Shinohara S 2008 *Proc. Int. Congress on Plasma Physics (Fukuoka, Japan)* FA.P2-004
[24] Shamrai K P, Shinohara S, Virko V F, Kirichenko G S, Slobodyan V M and Virko Yu V 2005 *Plasma Phys. Control. Fusion* **47** A307
[25] Chen F F 1991 *Plasma Phys. Control. Fusion* **33** 339
[26] Chen F F 1984 *Introduction to Plasma Physics and Controlled Fusion* 2nd edn (New York: Plenum)
[27] Miyamoto K 1989 *Plasma Physics for Nuclear Fusion* (Cambridge, MA: MIT Press)